VOL. 15, NO. 10, MAY 2020 ISSN 1819-6608
ARPN Journal of Engineering and Applied Sciences

www.arpnjournals.com

TWO-PHASE NONLINEAR RHEOLOGICAL ANALYSIS OF BLOOD FLOW IN SMALL DIAMETER BLOOD VESSELS WITH CONSTRICTION

Afiqah Wajihah S and D S Sankar
School of Applied Sciences and Mathematics, Universiti Teknologi Brunei, Jalan Tungku Link, Gadong, BA, Brunei Darussalam
E-Mail: duraisamy.sankar@utb.edu.bn

ABSTRACT

The two-phase flow of blood in a small diameter blood vessel under mild stenotic condition is investigated in this mathematical analysis, modelling the densely concentrated red cells in the inner phase region as Herschel-Bulkley fluid and the plasma with depleted red cells in the peripheral phase region as Newtonian fluid. The analytic solutions for the velocity profile, rate of flow, slip velocity, shear stress at the blood vessel's wall, resistive impedance to flow and core fluid's viscosity are obtained. It is found that when the stenosis length ratio and the flow index parameter increase, the slip velocity increases significantly and an opposite behavior is noticed for the core fluid's viscosity. It is also recorded that the percentage of difference between the core fluid's viscosity in the two-phase Herschel-Bulkley fluid model and the corresponding experimental values in the blood vessel's of diameter $40\ \mu m$ and $66.6\mu m$ are found to be 1.27% and 0.32% respectively and the respective differences observed by Ponalagausamy and Tamil Selvi (2011) in their two-layered Casson fluid model are 3.75% and 6.86% respectively. The estimated slip velocity values of two-phase Herschel-Bulkley fluid model in the blood vessels of diameter $40\ \mu m$ and $66.6\mu m$ are recoded as 1.202 *cm/s* and 0.7405 *cm/s* respectively and these values are in good alignment with the respective values obtained by Ponalagusamy and Tamil Selvi (2011) for two-fluid Casson model. The estimates of the core fluid's viscosity in two-phase Herschel-Bulkley fluid model increase gradually when the flow index parameter increases in the blood vessels of diameter $40\ \mu m$ and this behavior is reversed in the blood vessels of diameter $66.6\mu m$.

Keywords: two-phase blood flow; herschel-bulkley fluid; slip velocity; core fluid's viscosity.

1. INTRODUCTION

Among the various diseases which severely affect people's health condition, cardiovascular diseases are the most serious diseases that claim millions of lives across the globe annually. The most commonly occurring cardiovascular diseases are the heart diseases which mainly occur due to the development of constrictions in the coronary arteries, pulmonary arteries, cerebrovascular arteries etc. [1]. The constrictions in the blood vessels are attributed by the progression of atherosclerotic plaques (by the deposit of fatty substances) that protrude into the lumen of the blood vessels and this is medically termed as stenosis [2]. The stenosis development passes through three stages. In the initial stage, it is very mild (obstructing about 10% - 20% of cross-sectional area of the blood vessel) and the flow remains laminar, whereas when it progress to stage 2 (constricts around 25% - 40% of the blood vessel's cross-sectional area), the flow is still laminar, but back flow occurs in the neighboring region of stenosis. When the stenosis development reaches stage 3 (when the constriction in the blood vessel exceeds 50% of its cross-sectional area), the blood flow becomes turbulent [3, 4]. The most serious consequence of arterial stenosis is the increased flow resistance in the downstream of the artery and thus it reduces the blood supply to various parts of the body which could cause serious diseases, for example, the coronary arterial stenosis may cause heart attack, reduction of blood supply in the cerebral arteries that could lead to ischemic stroke which results in behavioral change of the subject, numbness, paralysis attack, speech difficulties etc. [5, 6]. Hence, the investigation on the flow of blood through arterial stenosis is very important not only to understand the major changes caused by stenosis in the rheological behavior of blood such as shear stress at the wall of the artery, velocity profile, frictional resistance to flow etc., but also for the diagnosis and treatment of several cardiovascular diseases [7].

It is well accepted that blood is the constitution of mainly three types of corpuscles, namely leukocytes, erythrocytes and thrombocytes in the aqueous solution, namely the plasma (composition of proteins and water) [8]. Leukocytes (white cells) are relatively large in size ($12-15\mu m$) and less in population ($7000-8000/cm^3$ of blood) which plays a vital role to maintain the immune system in our body, whereas erythrocytes (red cells) are relatively smaller in size ($6-8\mu m$) compared to leukocytes, but they are very numerous in population ($5-5.5\ million/cm^3$ of blood in male and $4-4.5\ million/cm^3$ of blood in female) which carries oxygenated blood from the lungs to tissues and takes out carbon-dioxide from tissues to lungs to exhale from the body [9]. Thrombocytes (platelets) are smaller than erythrocytes in size and normally their population is ; $250,000/mm^3$ of blood. These play an important role in blood coagulation (the process of forming semisolid lumps in blood) and more platelets would be produced during and after injury [10].

Blood depicts abnormal character when it flows under different rheological conditions. When it flows at higher shear rate ($>50/s$) in larger diameter ($>300\mu m$)

blood vessels, it depicts Newtonian fluid's nature, whereas when it flows in narrow arteries (diameter $<300\mu m$) at low shear rate ($<50/s$), it delineates the character of non-Newtonian fluid [11]. In particular, in diseased state, it shows the noticeable behavior of non-Newtonian fluids [12]. Herschel-Bulkley (H-B) fluid is one of the non-Newtonian fluid models having non-zero yield stress which is often used to model the blood when it flows in smaller diameter arteries at lower shear rates [13]. Sankar and Ismail [14] spelt out that the residual variation (the sum of the squares of the deviations of experimental observations from the corresponding theoretical observations) of H-B fluid model is considerably lower than that of the Casson fluid model. Furthermore, H-B fluid model shall also be brought down to the fluid models of Power law, Bingham and Newtonian for the particular values of its parameters such as yield stress and flow index [15, 16]. Moreover, H-B fluid model can exhibit the character of shear thickening fluid when the flow index parameter value is less than unity and it depicts the behavior of shear thinning fluid when the flow index parameter value is greater than unity [17]. Hence, in lieu of the aforementioned advantageous of using H-B fluid model, it is suitable to model blood as H-B fluid when it flows in smaller diameter arteries at lower rate of shear, in particularly at the pathetic state (under stenotic conditions).

Srivastava and Saxena [18] reported that the modelling of blood by single-phase non-Newtonian fluid is not suitable when it flows in small diameter arteries at lower rate of shear; rather, it would be more suitable to model the blood as two-phase fluid model, treating the concentration of most of the red cells in the inner phase (core) region as non-Newtonian fluid and the red cell-depleted plasma in the outer phase (peripheral layer) region as Newtonian fluid. Many theoretical investigations modelled blood as two-phase fluid to analyze the influence of core fluid's viscosity, yield stress and peripheral layer thickness on the vital rheological quantities such as velocity profile, skin friction, frictional impedance to flow etc. [19, 20]. Since H-B fluid model has more relevance to model the blood (as pointed out earlier), it is very suitable to treat the thickly populated red cells in the inner phase region of the two-phase blood rheology as H-B fluid model.

Several researchers observed the fact that there exists slip velocity in blood flow at the artery wall [21, 22]. Santhosh *et al*. [23] and Zaman *et al*. [24] assumed the presence of slip velocity at the blood vessel's wall in their theoretical studies. Bhatnagar *et al*. [25] discussed the influence of slip velocity in blood rheology through arteries with complicated stenosis structures. Misra and Shit [26] mathematically analyzed the influence of slip velocity and various depth levels of stenosis on rate of flow, friction at the artery wall and frictional impedance to blood flow. Sankar and Lee [27] analyzed the influence of slip velocity in different kinds of flow of H-B fluid between parallel plates with applications to bio-fluid dynamics and industrial engineering. In lieu of the aforementioned evidences, it is well acceptable to incorporate the presence of slip velocity at the blood vessels' wall in the modelling of blood rheology.

The viscosity of core fluid in the two-phase flow of blood is a vital factor that influences the blood's rheological properties under normal and diseased state [28]. Wang and Bassingthwaighte [29] applied a two-fluid model to investigate the blood flow in curved artery and they utilized the experimental data of others to determine the peripheral thickness and also computed the ratio between the core fluid's viscosity and the plasma viscosity in the peripheral layer region. Ponnalagar Samy and Tamil Selvi [30] used the two-phase Caason fluid model to investigate the blood rheology in stenotic arteries and derived the expression for the slip velocity at the wall of the artery and the ratio between the core fluid viscosity and plasma's viscosity in the outer (peripheral) layer region. Recapping the many merits of using H-B fluid model rather than Casson fluid model for modelling blood flow, one can accept the fact that it would be more suitable to model the suspension of the concentrated red cells in the core region of the two-phase fluid model of blood as H-B fluid model rather than the Casson fluid model. Hence, in this mathematical analysis, it is aimed to analyze the two-phase fluid flow of blood in small diameter blood vessel with mild symmetric stenosis, assuming the suspension of more concentrated red cells in the core region as H-B fluid and the cell-depleted plasma in the peripheral layer region as Newtonian fluid. The layout of this mathematical investigation is briefed as below:

Section 2 presents mathematical formulation of the flow problem and then non-dimensionalizes the momentum and constitutive equations.Boundary conditions pertaining to the flow problem are assumed and then dimensionalized in Section 2.Section 3 solves the system of nonlinear differential equations to obtain the analytic solutions to the velocity profile, skin friction, flow rate, slip velocity and viscosities of fluids in the inner phase region and outer phase region. Section 4 analyzes the influence of yield stress, flow index parameter, Reynolds number and stenosis length ratio on these flow quantities with the help of graphical and tabular representation of data. The concluding Section 5 lists out the major findings of this study.

2. MATHEMATICAL FORMULATION

2.1 Governing Equations

Let us study the two-phase, laminar, axi-symmetric, steady and fully developed uni-directional flow of blood in the axial direction in a small diameter artery with mild constriction, modelling the suspension of thickly populated red cells in the inner phase (core layer) region as Herschel-Bulkley (H-B) fluid and the red cell depleted plasma in the outer phase (peripheral layer) region as Newtonian fluid. The mild asymmetric shape of constriction present in the artery is assumed to be due to the development of stenosis in the inner wall of the artery.

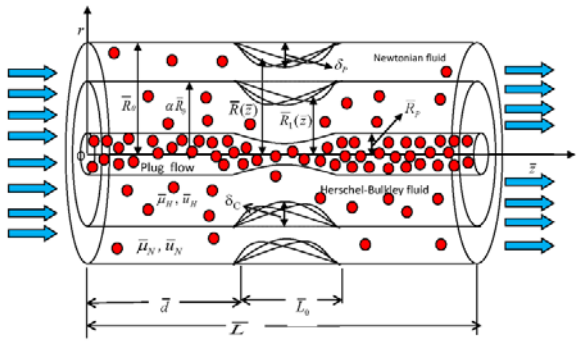

Figure-1. Geometry of tapered arterial segment with mild asymmetric stenosis.

The geometry of the arterial segment with mild asymmetric stenosis is depicted in Figure-1. As the blood vessels are cylindrical shaped, cylindrical polar coordinate system $\left(\bar{r},\bar{\phi},\bar{z}\right)$ is utilized to investigate the flow problem, where $\bar{r}$ and $\bar{z}$ denote the axes in the radial and axial directions respectively.

The geometry of the stenosis in the peripheral region is mathematically represented as

$$\bar{R}(\bar{z})/\bar{R}_0=\begin{cases}1-\bar{G}\left[\left(\bar{z}-\bar{d}\right)\bar{L}_0^{m-1}-\left(\bar{z}-\bar{d}\right)^m\right] & \text{if } \bar{z}\in\left(\bar{d},\bar{d}+\bar{L}_0\right)\\ 1 & \text{otherwise}\end{cases} \quad (1a)$$

where $\bar{G}=\left(\bar{\delta}_P/\bar{R}_0\bar{L}_0\right)m^{m/(m-1)}$, $\bar{\delta}_P$ is the maximum stenosis depth at $\bar{z}=\bar{L}_0/m^{m/(m-1)}+\bar{d}$ so that $\bar{\delta}_P/\bar{R}_0<<1$, $\bar{R}(\bar{z})$ is the artery radius in the stenotic region, $\bar{R}_0$ is the radius of the normal artery, $\bar{L}_0$ is the stenosis length, $\bar{d}$ denotes the starting point of stenosis, m indicates the stenosis shape parameter. When $m=2$, the shape of the stenosis is symmetric and when $m>2$, the shape of stenosis skews towards right hand side. The geometry of the stenotic artery in the inner phase region is given by

$$\bar{R}_1(\bar{z})/\bar{R}_0=\begin{cases}\alpha-\left[\left(\bar{z}-\bar{d}\right)\bar{L}_0^{m-1}-\left(\bar{z}-\bar{d}\right)^m\right]\bar{G} & \text{if } \bar{z}\in\left(\bar{d},\bar{d}+\bar{L}_0\right)\\ \alpha & \text{otherwise}\end{cases} \quad (1b)$$

where $\bar{R}_1\left(\bar{z}\right)$ is the artery radius in the stenosed inner phase region, α is the ratio of the central inner phase region to the normal artery radius, $\bar{\delta}_C$ is the maximum depth of the stenosis in the inner phase region such that $\left[\bar{\delta}_C/\bar{R}_0\right]<<1$.

The segment of blood vessel under investigation is considered as so long such that the entrance, end and special wall effects are negligibly small in magnitude and thus these are ignored in this study. Since the flow is assumed as slow, the inertial effects are neglected. We further assume that no body forces are acting on the fluid and the flow is due to the pressure gradient developed by the heart's pumping action. It is well accepted that for low Reynolds number viscous incompressible fluid flow, the radial component of the velocity is negligibly small and can be ignored. With the aforesaid assumptions, the momentum equations in the inner phase (core layer) region and outer phase (peripheral layer) region of the blood flow in the radial and axial directions reduce to the following equations respectively:

$$\frac{\partial\bar{p}}{\partial\bar{r}}=0;\quad \frac{1}{\bar{r}}\frac{\partial}{\partial\bar{r}}\left(\bar{r}\,\bar{\tau}_C\right)=-\frac{\partial\bar{p}}{\partial\bar{z}}, \quad (2a; 2b)$$

$$\frac{\partial\bar{p}}{\partial\bar{r}}=0;\quad \frac{1}{\bar{r}}\frac{\partial}{\partial\bar{r}}\left(\bar{r}\,\bar{\tau}_P\right)=-\frac{\partial\bar{p}}{\partial\bar{z}}, \quad (3a; 3b)$$

where $\bar{p}$ is the pressure in the fluid flow; $\bar{\tau}_C$, $\bar{\tau}_P$ are the shear stresses acting in the core region and peripheral layer region of blood flow. Eqs. (2a) and (3a) imply that the pressure is invariant along the radial direction and it varies only in the axial direction. The constitutive equation of H-B fluid and Newtonian fluid which represents the fluid in the core region and peripheral layer region are given below respectively [20]:

$$-\frac{\partial\bar{u}_C}{\partial\bar{r}}=\begin{cases}\dfrac{1}{\bar{\mu}_H}\left[\bar{\tau}_C-\bar{\tau}_y\right]^n, & \text{if } \bar{\tau}>\bar{\tau}_y\\ 0 & \text{if } \bar{\tau}\le\bar{\tau}_y\end{cases} \quad (4a)$$

$$-\frac{\partial\bar{u}_P}{\partial\bar{r}}=\frac{\bar{\tau}_P}{\bar{\mu}_P} \quad (4b)$$

where $\bar{u}_C,\bar{u}_P$ are the velocity of the fluid in the core region and peripheral layer region, $\bar{\tau}_y$ is the yield stress of H-B fluid; $\bar{\mu}_H,\bar{\mu}_P$ are the viscosity coefficients of the fluid in the core region and peripheral layer region and n is the flow index parameter which characterizes the fluid behavior. Eq. (4a) indicates that normal (shear) flow happens in the region where the shear stress exceed the yield stress limit and solid-like (plug) flow occurs in the region where the shear stress does not exceed the bench mark of yield stress value. When $\bar{\tau}_y=1$, Eq. (4a) reduces to the constitutive equation of Bingham fluid and when $\bar{\tau}_y=0$, Eq. (4b) reduces to the constitutive equation of Newtonian fluid. The following appropriate boundary and interface conditions applies to the present flow problem:

$$\bar{\tau}_C \text{ is finite at } \bar{r}=0;\quad \frac{\partial\bar{u}_C}{\partial\bar{r}}=0 \text{ at } \bar{r}=0;\quad \bar{u}_P=\bar{u}_S\left(\bar{z}\right) \text{ at } \bar{r}=\bar{R} \quad (5a; 5b; 5c)$$

$$\bar{\tau}_C=\bar{\tau}_P \text{ at } \bar{r}=\bar{R}_1;\quad \bar{u}_C=\bar{u}_P \text{ at } \bar{r}=\bar{R}_1. \quad (6a; 6b)$$

ARPN Journal of Engineering and Applied Sciences

Note that Eq. (5c) corresponds to the slip velocity at the blood vessel wall.

2.2 Non-Dimensionalization

We introduce the following non-dimensional variables:

$$r=\bar{r}/\bar{R}_0;\ R=\bar{R}/\bar{R}_0;\ R_1=\bar{R}_1/\bar{R}_0;\ z=\bar{z}/\bar{z}_0;\ u_C=\bar{u}_C/\bar{U}_0;\ u_P=\bar{u}_P/\bar{U}_0;$$
$$u_S=\bar{u}_S/\bar{U}_0;\ p=\bar{p}/\bar{\rho}_P\bar{U}_0^2;\ \tau_C=\bar{\tau}_C/\bar{\rho}_P\bar{U}_0^2;\ \tau_P=\bar{\tau}_P/\bar{\rho}_P\bar{U}_0^2;\ \theta=\bar{\tau}_y/\bar{\rho}_P\bar{U}_0^2;$$
$$\delta=\bar{\delta}/\bar{R}_0;\ L_0=\bar{L}_0/\bar{R}_0;\ \mu=\bar{\mu}_P/\bar{\mu}_C;\ Re_P=\bar{U}_0\bar{R}_0\,\bar{\rho}_P/\bar{\mu}_P \quad (7)$$

where $\bar{U}_0$ is the mean velocity of blood in the normal artery. It is to be noted that

$$\bar{\mu}_C=\bar{\mu}_H\Big/\left(\bar{\rho}_P\bar{U}_0^2\right)^{n-1} \quad (8a)$$

has physical dimension same as that of Newtonian fluid's viscosity and

$$\left[\bar{\mu}_H\right]=T\left(M/LT^2\right)^n. \quad (8b)$$

Using Eq. (2b) in Eq. (4a) and then applying the non-dimensional variables in the resulting equation, one can obtain

$$-\frac{\partial u_C}{\partial r}=\mu\, Re_P\left[\frac{1}{\beta}\left(\frac{q(z)r}{2}\right)-\theta\right]^n, \quad (9)$$

where $q(z)=-\partial p/\partial z$ and $\beta=\bar{z}_0/\bar{R}_0$. Applying Eq. (3b) in Eq. (4b) and then making use of the non-dimensional variables in the resulting equation, we obtain

$$-\frac{\partial u_P}{\partial r}=\frac{Re_P}{\beta}\left(\frac{q(z)r}{2}\right). \quad (10)$$

The dimensionless form of the boundary conditions (5) and (6) are

$$\tau_C \text{ is finite at } r=0;\ \frac{\partial u_C}{\partial r}=0 \text{ at } r=0;\ u_P=u_S(z) \text{ at } r=R \quad (11a;\ 11b;\ 11c)$$

$$\tau_C=\tau_P \text{ at } r=R_1;\qquad u_C=u_P \text{ at } r=R_1. \quad (12a;\ 12b)$$

3. METHOD OF SOLUTION

Integrating Eq. (10) and then making use of the boundary condition (11c), one can get the velocity of plasma in the peripheral layer region as

$$u_P(r,z)=\frac{\mathrm{Re}_P\, q(z)R^2}{4\beta}\left[1-\left(\frac{r}{R}\right)^2\right]+u_S(z). \quad (13)$$

where $q(z)=-dp/dz$. Expanding the RHS of Eq. (9) in binomial series and making three term approximation in it (by neglecting $(R_P/r)^4$ and higher powers of R_P/r as $R_P/r<1$ in $R_P\le r\le R_1$), one can get

$$-\frac{\partial u_C}{\partial r}=\mu Re_P\left(\frac{q(z)}{2\beta}\right)^n\left[r^n-nR_Pr^{n-1}+\frac{n(n-1)}{2}R_P^2r^{n-2}-\frac{n(n-1)(n-2)}{6}R_P^3r^{n-3}\right], \quad (14)$$

where $R_P=2\beta\left[\theta/q(z)\right]$. Integrating Eq. (14) and then making use of the interface boundary condition (12b) and peripheral layer velocity (obtained in Eq. (13)), the expression for velocity in the core region is obtained as

$$u_C(r,z)=\mu\,\mathrm{Re}_P\,R_1^{n+1}\left(\frac{q(z)}{2\beta}\right)^n\left[\frac{1}{(n+1)}\left\{1-\left(\frac{r}{R_1}\right)^{n+1}\right\}-\left(\frac{R_p}{R_1}\right)\left\{1-\left(\frac{r}{R_1}\right)^{n}\right\}\right.$$
$$\left.+\frac{n}{2}\left(\frac{R_p}{R_1}\right)^2\left\{1-\left(\frac{r}{R_1}\right)^{n-1}\right\}-\frac{n(n-1)}{6}\left(\frac{R_p}{R_1}\right)^3\left\{1-\left(\frac{r}{R_1}\right)^{n-2}\right\}\right]+\frac{\mathrm{Re}_P\,q(z)R^2}{4\beta}\left\{1-\left(\frac{r}{R_1}\right)^2\right\}+u_S(z) \quad (15)$$

From Eq. (15), the plug flow velocity u_{pl} can be obtained as below:

$$u_{pl}(z)=\mu Re_P\,R_1^{n+1}\left(\frac{q(z)}{2\beta}\right)^n\left[\left[\frac{1}{(n+1)}-\left(\frac{R_p}{R_1}\right)+n\left(\frac{R_p}{R_1}\right)^2-\frac{n(n-1)}{6}\left(\frac{R_p}{R_1}\right)^3+\frac{n(n-1)(n-2)}{6(n+1)}\left(\frac{R_p}{R_1}\right)^{n+1}\right]\right.$$
$$+\frac{Re_P\,q(z)R^2}{4\beta}\left\{1-\left(\frac{R_P}{R_1}\right)^2\right\}+u_S(z) \quad (16)$$

One can obtain the expression for flow rate in the peripheral layer region, core region and plug flow region as below respectively:

$$Q_P=2\int_{R_1}^{R}r\;u_P(r,z)\;dr\;=\frac{Re_P\,q(z)R^4}{8\beta}\left[1-\left(\frac{R_1}{R}\right)^2\right]^2+u_S(z)R^2\left[1-\left(\frac{R_1}{R}\right)^2\right] \quad (17)$$

$$Q_C = 2\int_{R_P}^{R_1} r\ u_C(r,z)\ dr \quad = 2\mu\, Re_P R_1^{n+3}\left(\frac{q(z)}{2\beta}\right)^n \left[\frac{1}{2(n+1)} - \frac{n}{2(n+2)}\left(\frac{R_p}{R_1}\right) + \frac{(n-2)}{4}\left(\frac{R_p}{R_1}\right)^2\right.$$
$$\left. -\frac{(n-4)(n+1)}{12}\left(\frac{R_p}{R_1}\right)^3 - \frac{n}{4}\left(\frac{R_p}{R_1}\right)^4 + \frac{n(n-1)}{12}\left(\frac{R_p}{R_1}\right)^5 - \frac{n(n^2+n-5)}{6(n+2)(n+3)}\left(\frac{R_p}{R_1}\right)^{n+3}\right]$$
$$+\frac{Re_P\ q(z)R^4}{4\beta}\left[\left(\frac{R_1}{R}\right)^2 - \left(\frac{R_p}{R}\right)^2 - \left(\frac{R_1}{R}\right)^4 + \left(\frac{R_1}{R}\right)^2\left(\frac{R_p}{R}\right)^2\right] + u_S(z)R_1^2\left[1-\left(\frac{R_p}{R_1}\right)^2\right] \tag{18}$$

$$Q_{pl} = 2\int_0^{R_P} r\ u_P(z)\ dr \quad = \mu\, Re_P R_1^{n+3}\left(\frac{q(z)}{2\beta}\right)^n \left[\frac{1}{(n+1)}\left(\frac{R_p}{R_1}\right)^2 - \left(\frac{R_p}{R_1}\right)^3 + n\left(\frac{R_p}{R_1}\right)^4 - \frac{n(n-1)}{6}\left(\frac{R_p}{R_1}\right)^5\right.$$
$$\left. -\frac{n(n-1)(n-2)}{6(n+1)}\left(\frac{R_p}{R_1}\right)^{n+3}\right] + \frac{Re_P\ q(z)R^4}{4\beta}\left[\left(\frac{R_P}{R}\right)^2 - \left(\frac{R_1}{R}\right)^2\left(\frac{R_p}{R}\right)^2\right] + u_S(z)R_P^2 \tag{19}$$

From Eqs. (17) - (19), one can obtain the simplified expression for the volumetric flow rate as

$$Q = R^2 u_S(z) - \frac{R_1^4 Re_P\ q(z)}{8\beta} + \mu\, Re_P R_1^{n+3}\left(\frac{q(z)}{2\beta}\right)^n F_1(n, R_1, R_p) \tag{20}$$

where

$$F_1(n, R_1, R_P) = \frac{1}{(n+3)} - \frac{n}{(n+2)}\left(\frac{R_p}{R_1}\right) + \frac{n(n-1)}{4(n+1)}\left(\frac{R_p}{R_1}\right)^2$$
$$-\frac{(n^2-3n+2)}{6}\left(\frac{R_p}{R_1}\right)^3 + \frac{n}{2}\left(\frac{R_p}{R_1}\right)^4 - \frac{(n^2-9n-4)}{6(n+1)}\left(\frac{R_p}{R_1}\right)^{n+3}. \tag{21}$$

Eq. (20) can be expressed as an implicit equation for the pressure gradient $q(z)$ as below:

$$\frac{\mu\, \mathrm{Re}_p\ R_1^{n+3} F_1(n, R_1, R_p)}{(2\beta)^n}[q(z)]^n - \frac{R_1^4\ \mathrm{Re}_p}{8\beta}[q(z)] + R^2 U_S(z) - Q = 0 \tag{22}$$

Eq. (22) can be solved numerically for $q(z)$ using Newton's method. Using the numerical solution of $q(z)$ and numerical integration, one can get the resistive impedance to flow from the following formula:

$$\lambda = \frac{\Delta P}{Q} = \int_0^L \frac{q(z)}{Q}\, dz\,. \tag{23}$$

One can make use of the numerical solution of $q(z)$ (obtained from Eq. (22)) in the following formula to compute the wall shear stress:

$$\tau_w = \frac{1}{Re_P}\left(\frac{\partial u_P}{\partial r}\right)_{r=R} = -\frac{Re_P\ q(z)R}{2\beta} \tag{24}$$

3.1 Slip Velocity, Viscosity of Core Fluid and Outer Layer Thickness for Flow in Stenosed Artery

The studies of Brunn [31] propounded that the insertion of a thin film of solvent near the artery wall causes the fluid slip at the wall of the blood vessel. For one layered model $(\mu = 1,\ R_1 = R)$ with slip at the wall, one can get the expression for the volumetric flow rate Q_{1L} as given below:

$$Q_{1L} = R^2 u_S(z) - \frac{\rho^* R^4 Re\ q(z)}{8\beta} + \rho^* Re\, R^{n+3}\left(\frac{q(z)}{2\beta}\right)^n$$
$$\times\left[\frac{1}{(n+3)} - \frac{n}{(n+2)}\left(\frac{R_p}{R}\right) + \frac{n(n-1)}{4(n+1)}\left(\frac{R_p}{R}\right)^2 - \frac{(n^2-3n+2)}{6}\left(\frac{R_p}{R}\right)^3 + \frac{n}{2}\left(\frac{R_p}{R}\right)^4 - \frac{(n^2-9n-4)}{6(n+1)}\left(\frac{R_p}{R}\right)^{n+3}\right] \tag{25}$$

where $\rho^* = \bar{\rho}_P/\bar{\rho}$; $\mathrm{Re} = \bar{\rho}\,\bar{U}_0\ \bar{R}_0/\bar{\mu}^*$ and $\bar{\rho}$ and $\bar{\mu}^*$ are the density and viscosity of the fluid when the flow is considered as single layered. In the case of two-layered model without slip at the wall of the artery, the expression for the flow rate reduces to the following form:

$$Q_{2L} = -\frac{R^4 Re_P\ q(z)}{8\beta}\left(1-\frac{\delta(z)}{R}\right)^4 + \mu\, Re_P R^{n+3}\left(\frac{q(z)}{2\beta}\right)^n \left[\frac{1}{(n+3)}\left(1-\frac{\delta(z)}{R}\right)^{n+3}\right.$$
$$+\frac{n(n-1)}{4(n+1)}\left(\frac{R_p}{R}\right)\left(1-\frac{\delta(z)}{R}\right)^{n+2} + \frac{n(n-1)}{4(n+1)}\left(\frac{R_p}{R}\right)^2\left(1-\frac{\delta(z)}{R}\right)^{n+1} - \frac{(n^2-3n+2)}{6}\left(\frac{R_p}{R}\right)^3\left(1-\frac{\delta(z)}{R}\right)^n$$

$$+\frac{n}{2}\left(\frac{R_p}{R}\right)^4\left(1-\frac{\delta(z)}{R}\right)^{n-1}-\frac{\left(n^2-9n-4\right)}{6(n+1)}\left(\frac{R_p}{R}\right)^{n+3}\Bigg] \quad (26)$$

where $R_1 = R\left(1-\delta(z)/R\right)$. Since the two-phase fluid model without slip at the wall and single-phase fluid model with slip at the wall profound the same physical phenomena, the corresponding flow rates must be equal. Hence, equating the flow rates obtained in Eqs. (25) and (26), one can get the following expression for the slip velocity:

$$u_S(z) = -\frac{R^2 q(z)}{8\beta}\left[Re_P\left(1-\frac{\delta(z)}{R}\right)^2-\rho^* Re\right]+\left(\frac{q(z)}{2\beta}\right)^n R^{n+1}\left[\frac{1}{(n+3)}\left\{\mu\, Re_P\left(1-\frac{\delta(z)}{R}\right)^{n+1}-\rho^* Re\right\}\right.$$
$$-\frac{n}{(n+2)}\left(\frac{R_P}{R}\right)\left\{\mu\, Re_P\left(1-\frac{\delta(z)}{R}\right)^{n}-\rho^* Re\right\}+\frac{n(n-1)}{4(n+1)}\left(\frac{R_P}{R}\right)^2\left\{\mu\, Re_P\left(1-\frac{\delta(z)}{R}\right)^{n-1}-\rho^* Re\right\}$$
$$-\frac{\left(n^2-3n+2\right)}{6}\left(\frac{R_P}{R}\right)^3\left\{\mu\, Re_P\left(1-\frac{\delta(z)}{R}\right)^{n-2}-\rho^* Re\right\}+\frac{n}{2}\left(\frac{R_P}{R}\right)^4\left\{\mu\, Re_P\left(1-\frac{\delta(z)}{R}\right)^{n-3}-\rho^* Re\right\}$$
$$\left.-\frac{\left(n^2-9n-4\right)}{6(n+1)}\left(\frac{R_P}{R}\right)^{n+3}\left\{\mu\, Re_P-\rho^* Re\right\}\right] \quad (27)$$

If the flow rate is fixed, then Eq. (26) can be resolved for the core fluid's viscosity as below:

$$\bar{\mu}_C = \frac{\left\{\bar{\mu}_P\, Re_P R^{n+3}\left(\frac{q(z)}{2\beta}\right)^n\right\}\left[\begin{array}{l}\frac{1}{(n+3)}\left(1-\frac{\delta(z)}{R}\right)^{n+3}-\frac{n}{(n+2)}\left(\frac{R_p}{R}\right)\left(1-\frac{\delta(z)}{R}\right)^{n+2}\\ +\frac{n(n-1)}{4(n+1)}\left(\frac{R_p}{R}\right)^2\left(1-\frac{\delta(z)}{R}\right)^{n+1}-\frac{\left(n^2-3n+2\right)}{6}\left(\frac{R_p}{R}\right)^3\left(1-\frac{\delta(z)}{R}\right)^{n}\\ +\frac{n}{2}\left(\frac{R_p}{R}\right)^4\left(1-\frac{\delta(z)}{R}\right)^{n-1}-\frac{\left(n^2-9n-4\right)}{6(n+1)}\left(\frac{R_p}{R}\right)^{n+3}\end{array}\right]}{\left\{Q^*+\frac{R^4\, Re_P\, q(z)}{8\beta}\left(1-\frac{\delta(z)}{R}\right)^4\right\}} \quad (28)$$

Since, the outer (peripheral) layer thickness $\delta(z)$ is an unknown quantity in Eqs. (27) and (28), we can find it using the following procedure. For the two-phase fluid flow without slip at the wall of the artery ($u_S = 0$), the analytic expression for velocity profile can be deduced from Eq. (15) as below:

$$u_C(r,z) = \mu\, Re_P\, R^{n+1}\left(\frac{q(z)}{2\beta}\right)^n\left[\frac{1}{(n+1)}\left\{\left(1-\frac{\delta(z)}{R}\right)^{n+1}-\left(\frac{r}{R}\right)^{n+1}\right\}-\left(\frac{R_p}{R}\right)\left\{\left(1-\frac{\delta(z)}{R}\right)^{n}-\left(\frac{r}{R}\right)^{n}\right\}\right.$$
$$\left.+\frac{n}{2}\left(\frac{R_p}{R}\right)^2\left\{\left(1-\frac{\delta(z)}{R}\right)^{n-1}-\left(\frac{r}{R}\right)^{n-1}\right\}-\frac{n(n-1)}{6}\left(\frac{R_p}{R}\right)^3\left\{\left(1-\frac{\delta(z)}{R}\right)^{n-2}-\left(\frac{r}{R}\right)^{n-2}\right\}\right]$$
$$+\frac{\mathrm{Re}_P\, q(z) R^2}{4\beta}\left\{1-\left(1-\frac{\delta(z)}{R}\right)^2\right\} \quad (29)$$

From Eq. (29), one can get the centerline velocity (velocity at the plug core radius) as below:

$$U = \mu\, Re_P\, R^{n+1}\left(\frac{q(z)}{2\beta}\right)^n\left[\frac{1}{(n+1)}\left(1-\frac{\delta(z)}{R}\right)^{n+1}-\left(\frac{R_p}{R}\right)\left(1-\frac{\delta(z)}{R}\right)^{n}+\frac{n}{2}\left(\frac{R_p}{R}\right)^2\left(1-\frac{\delta(z)}{R}\right)^{n-1}\right.$$

$$-\frac{n(n-1)}{6}\left(\frac{R_p}{R}\right)^3\left(1-\frac{\delta(z)}{R}\right)^{n-2}+\frac{n(n-1)(n-2)}{6(n+1)}\left(\frac{R_P}{R}\right)^{n+1}\Bigg]+\frac{\mathrm{Re}_P\, q(z)R^2}{4\beta}\left\{1-\left(1-\frac{\delta(z)}{R}\right)^2\right\} \tag{30}$$

Elimination of μ from Eqs. (26) and (30) yields the following equation:

$$\begin{aligned}
&\frac{UR^2}{(n+3)}\left(1-\frac{\delta(z)}{R}\right)^{n+3}+\frac{UR^2 n(n-1)}{4(n+1)}\left(\frac{R_p}{R}\right)\left(1-\frac{\delta(z)}{R}\right)^{n+2}-\left\{\frac{(n-1)}{2}\left(\frac{R_p}{R}\right)^2+\frac{Q^*}{(n+1)}\right\}\left(1-\frac{\delta(z)}{R}\right)^{n+1}\\
&-\left\{\frac{(n^2-3n+2)UR^2}{6}\left(\frac{R_p}{R}\right)^2-Q^*\right\}\left(\frac{R_p}{R}\right)\left(1-\frac{\delta(z)}{R}\right)^{n}+\left\{UR^2\left(\frac{R_p}{R}\right)^2-Q^*\right\}\left(\frac{n}{2}\right)\left(\frac{R_p}{R}\right)^2\left(1-\frac{\delta(z)}{R}\right)^{n-1}\\
&-\frac{Q^* n(n-1)}{6}\left(\frac{R_p}{R}\right)^3\left(1-\frac{\delta(z)}{R}\right)^{n-2}+\frac{Q^* n(n-1)(n-2)}{6(n+1)}\left(\frac{R_p}{R}\right)^{n+1}-\frac{UR^2(n^2-9n-4)}{6(n+1)}\left(\frac{R_p}{R}\right)^{n+3}\\
&+\frac{Re_P\, q(z)R^4}{4\beta}\Bigg[\frac{(n-1)}{2(n+1)(n+3)}\left(1-\frac{\delta(z)}{R}\right)^{n+5}-\frac{(n^2+n+2)}{4(n+1)}\left(\frac{R_p}{R}\right)\left(1-\frac{\delta(z)}{R}\right)^{n+4}\\
&-\left\{\frac{(3n-2)}{4}\left(\frac{R_p}{R}\right)^2+\frac{1}{(n+3)}\right\}\left(1-\frac{\delta(z)}{R}\right)^{n+3}-\left\{\frac{(n^2-5n+4)}{12}\left(\frac{R_p}{R}\right)^2+\frac{n(n-1)}{4(n+1)}\right\}\left(\frac{R_p}{R}\right)\left(1-\frac{\delta(z)}{R}\right)^{n+2}\\
&+\left\{\frac{n}{2}\left(\frac{R_p}{R}\right)^2+\frac{(n-1)}{2}\right\}\left(\frac{R_p}{R}\right)^2\left(1-\frac{\delta(z)}{R}\right)^{n+1}+\frac{(n-1)(n-2)}{6}\left(\frac{R_p}{R}\right)^3\left(1-\frac{\delta(z)}{R}\right)^{n}-\frac{n}{2}\left(\frac{R_p}{R}\right)^4\left(1-\frac{\delta(z)}{R}\right)^{n-1}\\
&+\frac{n(n-1)(n-2)}{12(n+1)}\left(\frac{R_p}{R}\right)^{n+1}\left(1-\frac{\delta(z)}{R}\right)^4-\frac{(n^2-9n-4)}{6(n+1)}\left(\frac{R_p}{R}\right)^{n+3}\left(1-\frac{\delta(z)}{R}\right)^2\Bigg]=0
\end{aligned} \tag{31}$$

As all the quantities in Eq. (31) except $\delta(z)$ can be computed in *vitro*, the peripheral layer thickness $\delta(z)$ can be computed numerically by Newton-Raphson method. Once the numerical value of the peripheral layer thickness $\delta(z)$ is computed numerically, one can obtain the values of $\bar{u}_S(\bar{z})$ and $\bar{\mu}_C$ from Eqs. (27) and (28).

3.2 Slip Velocity, Core Fluid's Viscosity and Outer Layer Thickness for Flow in Normal Artery

For blood flow through normal tube (without stenosis), the dimensional form of the expression for slip velocity, core fluid's viscosity coefficient and outer (peripheral) layer thickness are obtained from Eqs. (27), (28) and (31) (by making use of the Eq. (7)) and the simplified form of these expressions are presented hereunder respectively:

$$\begin{aligned}
\bar{u}_S=&-\frac{\bar{R}_0^2\,\bar{q}_0}{8}\left[\frac{1}{\bar{\mu}_P}\left(1-\frac{\bar{\delta}_0}{\bar{R}_0}\right)^2-\frac{1}{\bar{\mu}^*}\right]+\left(\frac{\bar{q}_0}{2}\right)^n\bar{R}_0^{n+1}\Bigg[\frac{1}{(n+3)}\left[\frac{1}{\bar{\mu}_C}\left(1-\frac{\bar{\delta}_0}{\bar{R}_0}\right)^{n+1}-\frac{1}{\bar{\mu}^*}\right]\\
&-\frac{n}{(n+2)}\left(\frac{\bar{R}_P}{\bar{R}_0}\right)\left[\frac{1}{\bar{\mu}_C}\left(1-\frac{\bar{\delta}_0}{\bar{R}_0}\right)^{n}-\frac{1}{\bar{\mu}^*}\right]+\frac{n(n-1)}{4(n+1)}\left(\frac{\bar{R}_P}{\bar{R}_0}\right)^2\left[\frac{1}{\bar{\mu}_C}\left(1-\frac{\bar{\delta}_0}{\bar{R}_0}\right)^{n-1}-\frac{1}{\bar{\mu}^*}\right]\\
&-\frac{(n^2-3n+2)}{6}\left(\frac{\bar{R}_P}{\bar{R}_0}\right)^3\left[\frac{1}{\bar{\mu}_C}\left(1-\frac{\bar{\delta}_0}{\bar{R}_0}\right)^{n-2}-\frac{1}{\bar{\mu}^*}\right]+\frac{n}{2}\left(\frac{\bar{R}_P}{\bar{R}_0}\right)^4\left[\frac{1}{\bar{\mu}_C}\left(1-\frac{\bar{\delta}_0}{\bar{R}_0}\right)^{n-3}-\frac{1}{\bar{\mu}^*}\right]\\
&-\frac{(n^2-9n-4)}{6(n+1)}\left(\frac{\bar{R}_P}{\bar{R}_0}\right)^{n+3}\left[\frac{1}{\bar{\mu}_C}-\frac{1}{\bar{\mu}^*}\right]\Bigg]
\end{aligned} \tag{32}$$

ARPN Journal of Engineering and Applied Sciences

$$\bar{\mu}_H = \frac{\left\{\bar{\mu}_P\,\bar{R}_0^{n+3}\left(\bar{q}_0/2\right)^n\right\}\left[\begin{array}{l}\frac{1}{(n+3)}\left(1-\frac{\bar{\delta}_0}{\bar{R}_0}\right)^{n+3}-\frac{n}{(n+2)}\left(\frac{\bar{R}_p}{\bar{R}_0}\right)\left(1-\frac{\bar{\delta}_0}{\bar{R}_0}\right)^{n+2}\\ +\frac{n(n-1)}{4(n+1)}\left(\frac{\bar{R}_p}{\bar{R}_0}\right)^2\left(1-\frac{\bar{\delta}_0}{\bar{R}_0}\right)^{n+1}-\frac{\left(n^2-3n+2\right)}{6}\left(\frac{\bar{R}_p}{\bar{R}_0}\right)^3\left(1-\frac{\bar{\delta}_0}{\bar{R}_0}\right)^{n}\\ +\frac{n}{2}\left(\frac{\bar{R}_p}{\bar{R}_0}\right)^4\left(1-\frac{\bar{\delta}_0}{\bar{R}_0}\right)^{n-1}-\frac{\left(n^2-9n-4\right)}{6(n+1)}\left(\frac{\bar{R}_p}{\bar{R}_0}\right)^{n+3}\end{array}\right]}{\left\{\left(\bar{Q}^*\bar{\mu}_P/\pi\right)-\left(\bar{q}_0\bar{R}_0^4/8\right)\left(1-\left(\bar{\delta}_0/\bar{R}_0\right)\right)^4\right\}} \tag{33}$$

$$\begin{aligned}
&\frac{\bar{U}}{\bar{U}_0(n+3)}\left(1-\frac{\bar{\delta}_0}{\bar{R}_0}\right)^{n+3}+\frac{\bar{U}n(n-1)}{4\bar{U}_0(n+1)}\left(\frac{\bar{R}_p}{\bar{R}_0}\right)\left(1-\frac{\bar{\delta}_0}{\bar{R}_0}\right)^{n+2}-\left\{\frac{(n-1)}{2}\left(\frac{\bar{R}_p}{\bar{R}_0}\right)^2+\frac{Q^*}{\pi\bar{U}_0\bar{R}_0^2(n+1)}\right\}\left(1-\frac{\bar{\delta}_0}{\bar{R}_0}\right)^{n+1}\\
&-\left\{\frac{\bar{U}(n-1)(n-2)}{6\bar{U}_0}\left(\frac{\bar{R}_p}{\bar{R}_0}\right)^2-\frac{Q^*}{\pi\bar{U}_0\bar{R}_0^2}\right\}\left(\frac{\bar{R}_p}{\bar{R}_0}\right)\left(1-\frac{\bar{\delta}_0}{\bar{R}_0}\right)^{n}+\left\{\frac{\bar{U}}{\bar{U}_0}\left(\frac{\bar{R}_p}{\bar{R}_0}\right)^2-\frac{Q^*}{\pi\bar{U}_0\bar{R}_0^2}\right\}\left(\frac{n}{2}\right)\left(\frac{\bar{R}_p}{\bar{R}_0}\right)^2\left(1-\frac{\bar{\delta}_0}{\bar{R}_0}\right)^{n-1}\\
&-\left(\frac{\bar{Q}^*}{\pi\bar{U}_0\bar{R}_0^2}\right)\left(\frac{n(n-1)}{6}\right)\left(\frac{\bar{R}_p}{\bar{R}_0}\right)^3\left(1-\frac{\bar{\delta}_0}{\bar{R}_0}\right)^{n-2}+\left(\frac{\bar{Q}^*}{\pi\bar{U}_0\bar{R}_0^2}\right)\frac{n(n-1)(n-2)}{6(n+1)}\left(\frac{\bar{R}_p}{\bar{R}_0}\right)^{n+1}-\frac{\bar{U}\left(n^2-9n-4\right)}{6\bar{U}_0(n+1)}\left(\frac{\bar{R}_p}{\bar{R}_0}\right)^{n+3}\\
&+\frac{\bar{q}_0\,\bar{R}_0^2}{4\bar{\mu}_P\bar{U}_0}\left[\frac{(n-1)}{2(n+1)(n+3)}\left(1-\frac{\bar{\delta}_0}{\bar{R}_0}\right)^{n+5}-\frac{\left(n^2+n+2\right)}{4(n+1)}\left(\frac{\bar{R}_p}{\bar{R}_0}\right)\left(1-\frac{\bar{\delta}_0}{\bar{R}_0}\right)^{n+4}\right.\\
&-\left\{\frac{(3n-2)}{4}\left(\frac{\bar{R}_p}{\bar{R}_0}\right)^2+\frac{1}{(n+3)}\right\}\left(1-\frac{\bar{\delta}_0}{\bar{R}}\right)^{n+3}-\left\{\frac{(n-1)(n-4)}{12}\left(\frac{\bar{R}_p}{\bar{R}_0}\right)^2+\frac{n(n-1)}{4(n+1)}\right\}\left(\frac{\bar{R}_p}{\bar{R}_0}\right)\left(1-\frac{\bar{\delta}_0}{\bar{R}_0}\right)^{n+2}\\
&+\left\{\frac{n}{2}\left(\frac{\bar{R}_p}{\bar{R}_0}\right)^2+\frac{(n-1)}{2}\right\}\left(\frac{\bar{R}_p}{\bar{R}_0}\right)^2\left(1-\frac{\bar{\delta}_0}{\bar{R}_0}\right)^{n+1}+\frac{(n-1)(n-2)}{6}\left(\frac{\bar{R}_p}{\bar{R}_0}\right)^3\left(1-\frac{\bar{\delta}_0}{\bar{R}_0}\right)^{n}-\frac{n}{2}\left(\frac{\bar{R}_p}{\bar{R}_0}\right)^4\left(1-\frac{\bar{\delta}_0}{\bar{R}_0}\right)^{n-1}\\
&\left.+\frac{n(n-1)(n-2)}{12(n+1)}\left(\frac{\bar{R}_p}{\bar{R}_0}\right)^{n+1}\left(1-\frac{\bar{\delta}_0}{\bar{R}_0}\right)^4-\frac{\left(n^2-9n-4\right)}{6(n+1)}\left(\frac{\bar{R}_p}{\bar{R}_0}\right)^{n+3}\left\{1+\left(1-\frac{\bar{\delta}_0}{\bar{R}_0}\right)^2\right\}\right]=0
\end{aligned} \tag{34}$$

4. RESULTS AND DISCUSSIONS

The prime focus of this mathematical analysis is to investigate the influence of Reynolds number Re_P, flow index parameter n, yield stress θ, maximum depth of stenosis in the outer (peripheral) layer region δ_P, length ratio parameter β of stenosis, shape parameter m of stenosis and radius of inner phase region R_1 on the rheological quantities such as skin friction, velocity profile, flow rate, viscosity of the fluid in the core region, frictional resistance, peripheral layer thickness etc. through appropriate graphical and tabular representation of data which are obtained by evaluating the expressions of flow quantities using MATLAB program. The stenosis length in the arterial segment is assumed as $L_0 = 8$ and the initial location of the stenosis is assumed as $d = 0$, so that it lies between $z = 0$ and $z = 8$. The range of parameters used in this analysis is given below:

Stenosis depth δ_P: 0.1- 0.3; Shape of stenosis m: 2-8; Radius of core region R_1: 0.9 – 0.975; Stenosis length ratio β: 2-8; Yield stress θ: 0.1- 0.2; Flow index n : 0.95 - 1.35; Reynolds number Re_p: 0.05 –50.

4.1 Velocity Profiles

Figure-2 depicts the effect of the stenosis length ratio β on the plug flow velocity for different values of n and Re_P with $z = 4, m = 2, \mu = 0.4, \theta = 0.15$ and $\delta_p = 0.1$. One can notice that the plug flow velocity slowly increases when the stenosis length ratio β increases from 2 to 5 and then it rapidly increases when the stenosis length ratio β increases from 5 to 8. Also, we observe that plug flow velocity increases with the increase of the Reynolds number Re_P and flow index parameter n, but this increase is appreciable when the Reynolds number Re_P rises and the increase in the plug flow velocity is substantial when the flow index parameter n rises.

The velocity profiles in the radial direction for distinct values of the parameters Re_P and n with $z = 4, \theta = 0.15$ and $m = 2$ are illustrated in Figure-3. The velocity of blood soars with the rise of the flow index parameter n when the Reynolds number Re_P is treated as invariable and for a fixed flow index parameter n value, it marginally rises with the increase of the Reynolds number Re_P. Figure-4 sketches the axial variation in slip velocity

for distinct m, n and β values with $\theta = 0.1, \delta_p = 0.05, \rho^* = 1.025$ and $Re = 0.0003$. When the stenosis shape parameter m value is fixed, the slip velocity rises rapidly with the rise of stenosis length ratio parameter β and it increases appreciably with the rise of the flow index parameter n. One can also notice that when the stenosis shape parameter rises and all the other parameters kept as constant, the slip velocity reduces from the onset of the stenosis till the greatest stenosis depth and it increases from the greatest stenosis depth till the end point of the stenosis. Figures 2 - 4 propound the effect of the parameters m, n, β and Re_P on the plug flow velocity, velocity profile and slip velocity in the flow of blood in constricted blood vessels.

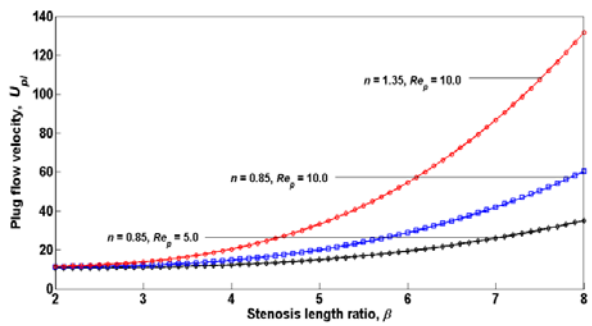

Figure-2. Effect of stenosis length ratio β on plug flow velocity for distinct values of n and Re_P with $z = 4, m = 2, \mu = 0.4, \theta = 0.15$ and $\delta_p = 0.1$.

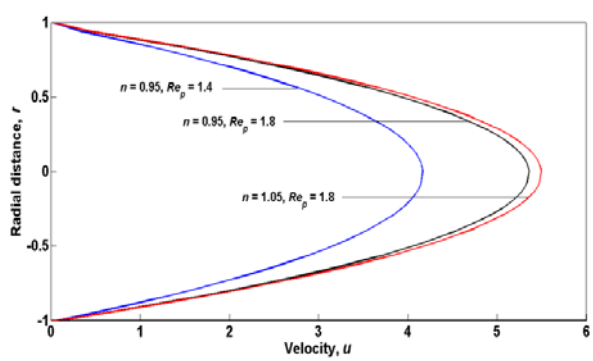

Figure-3. Velocity profiles for different values of n and Re_P with $z = 4, \theta = 0.15$ and $m = 2$.

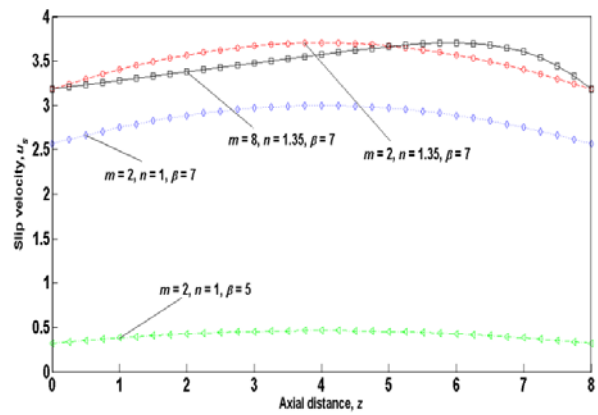

Figure-4. Axial variation of slip velocity for different values of m, n and β with $\theta = 0.1, \delta_P = 0.05$, $\rho^* = 1.025$ and $\mathrm{Re} = 0.0003$.

4.2 Flow Rate

The effect of the stenosis length ratio β on the flow rate for distinct values of δ_p and Re_P with $z = 4, U_S = 0.1, \mu = 0.4, R_1 = 0.95, m = 2, \theta = 0.1$ and $n = 0.95$ is delineated in Figure-5. It is observed that the rate of flow slowly rises when the stenosis length ratio β increases from 2 to 6 and then it soars (increases nonlinearly) when the stenosis length ratio β rises from 6 to 8. For a given value of the greatest stenosis depth δ_p, the rate of flow increases considerably with the rise of the Reynolds number Re_P and it rises very slightly with the increase of the stenosis depth δ_p when the Reynolds number Re_P is held constant.

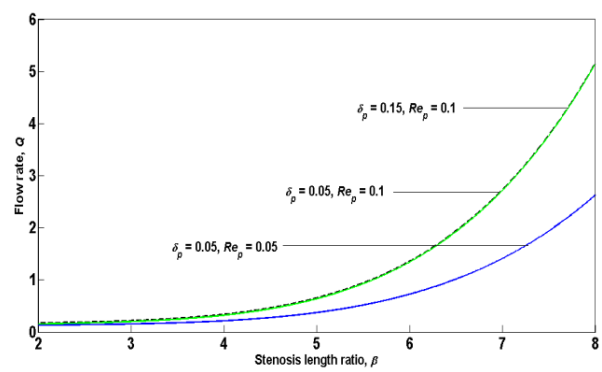

Figure-5. The effect of the stenosis length ratio β on the flow rate for distinct values of δ_p and Re_P with $z = 4, U_S = 0.1, \mu = 0.4, R_1 = 0.95, m = 2, \theta = 0.1$ and $n = 0.95$.

4.3 Wall Shear Stress

Figure-6 exhibits the influence of the stenosis length ratio β on the shear stress at the wall of the blood

vessel for distinct values of m and δ_P with $z = 4.4, \mu = 0.33, \theta = 0.1$ and $Re_p = 5$. One may observe that the shear stress at the blood vessel wall decreases rapidly (nonlinearly) with the rise of stenosis length ratio β from 2 to 6 and then it slowly decreases with the further rise of the stenosis length ratio from 6 to 8. Moreover, the wall shear stress in blood flow decreases slightly with the rise of the stenosis shape parameter m and it increases significantly with the rise of the maximum stenosis depth δ_P while the rest of the parameters were treated as invariants. The variation of wall shear stress with stenosis length ratio β for distinct yield stress θ values with $z = 4, m = 2, \mu = 0.4$ and $Re_p = 10$ is exhibited in Figure-7. One may propound that the wall shear stress increases significantly with the increase of the yield stress of blood.

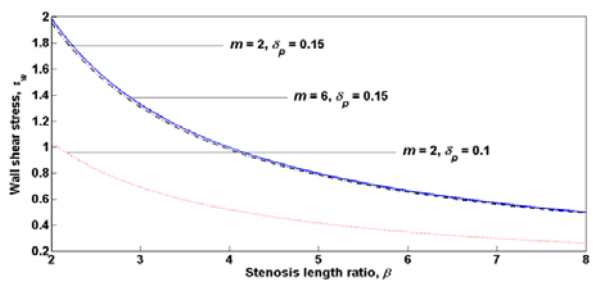

Figure-6. Influence of the stenosis length ratio β on the shear stress at the wall of the blood vessel for distinct values of m and δ_P with $z = 4.4, \mu = 0.33, \theta = 0.1$ and $Re_p = 5$.

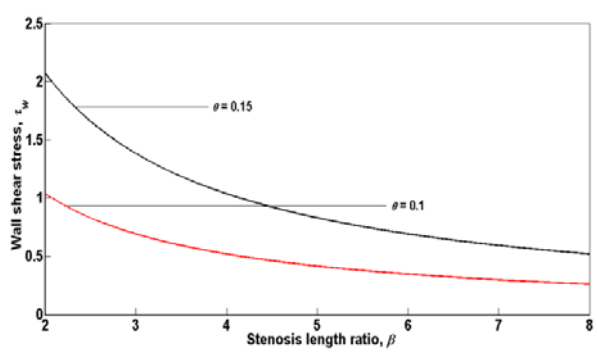

Figure-7. Variation of wall shear stress with stenosis length ratio β for different values of θ with $z = 4, m = 2, \mu = 0.4$ and $Re_p = 10$.

4.4 Core Fluid's Viscosity

Figure-8 limned the effect of yield stress θ on the core fluid's viscosity for distinct values of n and β with $z = 4, \alpha = 0.2, U_S = 0, \mu = 0.33, Re_P = 50, m = 2, \delta_P = 0.05$ and $\mu_P = 0.015$. One can notice that the core fluid's viscosity increases linearly (slowly) with the rise of the yield stress θ from 0.1 to 0.15 and then it increases nonlinearly (rapidly) when the yield stress θ rises further from 0.15 to 0.2. When the flow index parameter n value is held constant, the core fluid's viscosity increases significantly with the rise of the stenosis length ratio β. Also, it is found that the viscosity of core fluid increases considerably when the flow index parameter n rises while the stenosis length ratio β is treated as invariant.

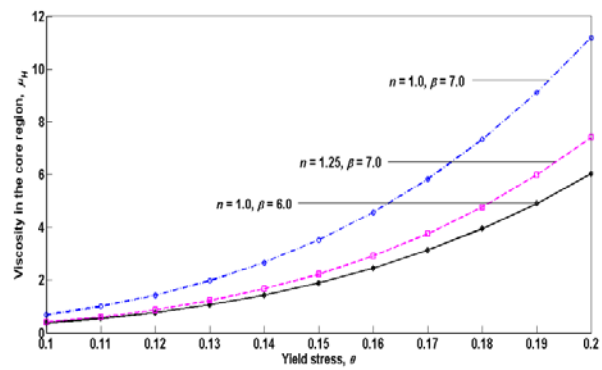

Figure-8. Effect of yield stress θ on the core fluid's viscosity for distinct values of n and β with $z = 4, \alpha = 0.2, U_S = 0, \mu = 0.33, Re_P = 50, m = 2, \delta_P = 0.05$ and $\mu_P = 0.015$.

4.5 Resistive Impedance To Flow

The axial variation of resistive impedance to flow for different values of stenosis shape parameter m with $\beta = 2, n = 1.25.0, \theta = 0.2, \delta_P = 0.2$ and $Re_p = 12$ is depicted in Figure-9. One may note that the impedance to flow rises rapidly in the axial direction from the onset of the stenosis $(z = 0)$ till the point of maximum stenosis depth and then it starts decreasing from the maximum stenosis depth till the end point of the stenosis $(z = 8)$. We also record that with the increase of the stenosis shape parameter m, the impedance to flow decreases appreciably in the first part of the stenosis (from the onset of the stenosis till maximum stenosis depth) and it rises considerably in the second part of the stenosis (from the maximum stenosis depth till the end point of the stenosis). Figure-10 shows the axial variation of flow impedance for distinct δ_p values with $\beta = 2, n = 1.5, \theta = 0.2, m = 2$ and $Re_p = 12$. One may note that the impedance to flow soars with the rise of the maximum stenosis depth while the rest of the flow parameters are treated as constants.

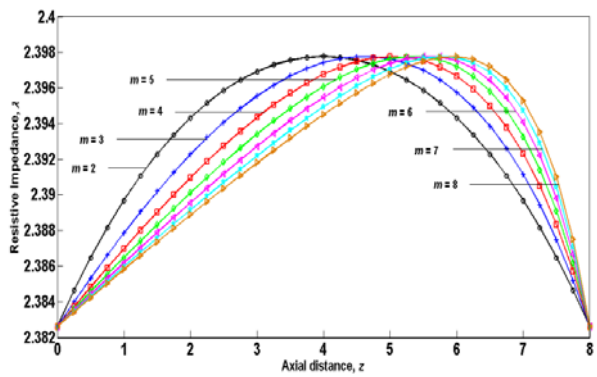

Figure-9. Axial variation in resistive impedance to flow for distinct m with $\beta = 2, n = 1.5, \theta = 0.2, \delta_p = 0.2$ and $Re_p = 12$.

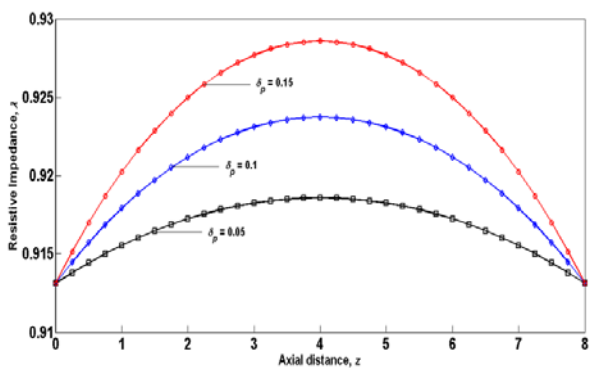

Figure-10. Axial variation in resistive impedance for distinct δ_p values with $\beta = 2, n = 1.5, m = 2, \theta = 0.2,$ and $Re_p = 12$.

4.6 Physiological Applications

The main goal of this study is not only to discuss some potential results, but also to render some possible physiological applications. To compare this study with the published results of other researchers and also to provide some possible clinical relevance of the present study, we make use of the clinical data that are given in Bugliarello and Hayden [32], Bugliarello and Sevilla [33] and Ponnalagar Samy and Tamil Selvi [30] and are listed in Table-1.

Table-2 makes use of the flow parameter values given in Table 1 to compute the core fluid's viscosity of two-phase H-B fluid model with $\mu = 0.33, \theta = 0.05,$ $\delta_p = 0.1, z = 4, m = 2, n = 0.55, R_p = 0.0004, R_0 = 0.004,$ and $\mu^* = 0.03$ and also it computes the percentage of difference between the core fluid's viscosity and the corresponding experimental values. Table-2 also compares this percentage of difference of core fluid's viscosity of two-phase Casson fluid model and the same experimental values. It is recorded that the percentage of difference obtained for two-phase H-B fluid model in $40\,\mu m$ and $66.6\,\mu m$ are 1.27% and 0.32%. The similar percentage of difference obtained by Ponnalagusamy and Tamil Selvi [30] for two-phase Casson fluid model in $40\,\mu m$ and $66.6\,\mu m$ are 3.75% and 6.86%. Thus, it is of important to note that the estimates of the percentage of the difference between the core fluid's viscosity of two-phase H-B fluid model and the corresponding experimental value are appreciably lower than the corresponding values obtained by Ponnalagusamy and Tamil Selvi [30] for two-phase Casson fluid model. Thus, the use two-phase H-B fluid model for blood flow modelling provides better accuracy in the computation of flow quantities when compared with the corresponding flow quantities provided by two-phase Casson fluid model and hence this comparison validates the present study.

Table-3 computes the core fluid's viscosity μ_H of two-phase H-B fluid flow for distinct values of flow index parameter n and blood vessel diameter (in μm). In the blood vessel of diameter either $40\,\mu m$ or $66.6\,\mu m$, the estimates of the core fluid's viscosity considerably increases with the increase of the flow index parameter n. One can also observe that in the two-phase fluid flow model of blood, the core fluid's viscosity decreases with the increase of the diameter of blood vessel. It is of important to note that the core fluid's viscosity obtained at $n = 0.52$ in $40\,\mu m$ blood vessel diameter and $n = 0.53$ in $66.6\,\mu m$ are in good agreement with the corresponding experimental values obtained by Ponnalagar Samy and Tamil Selvi [30] and this comparison further validates the present study.

Table-4 presents the estimated slip velocity values of two-phase H- B fluid flow in the blood vessels of diameter $40\,\mu m$ and $66.6\,\mu m$ and compares these values with the corresponding values of two-phase Casson fluid model [30]. One can note that the difference between the slip velocity values obtained for two-phase H-B fluid model and two-phase Casson fluid model are negligibly small. Thus, for a particular choice of the parameter values, two-phase H-B fluid model provides the same accuracy of results that are provided by two-phase Casson fluid model. Table-5 computes the estimated slip velocity values for different values of core fluid's viscosity and artery diameter with $z = 4, m = 2, R_0 = 0.004, R_p = 0.0004, \theta = 0.05, \delta_p = 0.1,$ $\mu = 0.33$ and $\mu^* = 0.05$. One can record that for the artery diameter $40\,\mu m$, the slip velocity decreases rapidly (nonlinearly) when the core fluid's viscosity rises. An opposite behavior in the slip velocity is noticed in the arteries of diameter $66.6\,\mu m$.

ARPN Journal of Engineering and Applied Sciences

Table-1. Clinical data of flow parameters (in dimensional form) for blood vessel diameters $40\,\mu m$ and $66.6\ \mu m$.

Flow Quantities	Blood vessels diameter $40\ \mu m$	Blood vessels diameter $66.6\,\mu m$
$\bar{Q}$	$0.192342\times10^{-4}\ cm^3/s$	$0.192342\times10^{-4}\ cm^3/s$
$\bar{q}_0$	$1675\times10^2\ dyne/cm^3$	$1675\times10^2\ dyne/cm^3$
$\bar{\mu}_P$	$0.0144P\ (\text{at } 25.5^\circ C)$	$0.0144P\ (\text{at } 25.5^\circ C)$
C	40%	40%
$\bar{\delta}_P$	$3.2\mu m$	$3.2\mu m$
$\bar{U}$	$2.37\,cm/s$	$2.37\,cm/s$
$\bar{\tau}_y$	$0.04\,dyne/cm^2$.	$0.04\,dyne/cm^2$

Table-2. Estimated values of core fluid's viscosity for two-phase H- B and Casson fluid models for blood vessels of different diameters with $z=4,\ m=2, n=0.55, R_p=0.0004,\ R_0=0.004, \mu=0.33, \theta=0.05, \delta_p=0.1$ and $\mu^*=0.03$.

Blood vessels diameter (μm)	Core fluid viscosity				
	Experimental values (A)	Two-phase H- B fluid model (B)	% of Difference (A) – (B)	Two-phase Casson fluid model (C)	% of Difference (A) – (C)
40	0.04244	0.0419	1.27	0.04403	3.75
66.6	0.01896	0.0189	0.32	0.02026	6.86

Table-3. Estimated Core fluid's viscosity in two-phase H-B fluid model for distinct values of flow index parameter n and blood vessel diameter (in μm) with $z=4, m=2, R_p=0.0004,\ \theta=0.05, \delta_p=0.1\ R_0=0.004, \mu=0.33,$ and $\mu^*=0.03$.

n / μm	0.45	0.46	0.47	0.48	0.49	0.5	0.51	0.52	0.53	0.54	0.55
40	0.0289	0.0305	0.0322	0.0339	0.0357	0.0377	0.0397	0.0424	0.0448	0.0470	0.0493
66.6	0.0147	0.0152	0.0157	0.0162	0.0167	0.0172	0.0178	0.0184	0.0189	0.0196	0.0202

Table-4. Estimated slip velocity values of two-phase H-B fluid model for different artery diameters with $z=4, m=2, R_0=0.004, R_p=0.0004, \mu=0.33, \delta_p=0.1, n=0.53,\ \theta=0.05,$ and $\mu^*=0.05$.

Artery diameter (μm)	Slip Velocity		
	Two-phase Casson fluid model (A)	Two-phase H-B fluid model (B)	Difference (A) - (B)
40	1.2101	1.202	0.0081
66.6	0.8108	0.7405	0.0703

Table-5. Estimated slip velocity (U_S) values for different values of core fluid's viscosity (μ_H) and artery diameters $40\ \mu m$ and $66.6\mu m$ with $z = 4, m = 2, R_0 = 0.004, \theta = 0.05, \delta_p = 0.1, R_p = 0.0004, \mu = 0.33$ and $\mu^* = 0.05$.

Artery diameter	μ_H	**0.0289**	**0.0305**	**0.0322**	**0.0339**	**0.0357**	**0.0377**	**0.0397**	**0.0419**
$40\ \mu m$	U_S	115.5	96.2	77.8	61.2	45.3	29.5	15.3	1.202
$66.6\mu m$	μ_H	0.0147	0.0152	0.0157	0.0162	0.0167	0.0172	0.0178	0.0184
	U_S	0.6179	0.6361	0.6530	0.6690	0.6840	0.6981	0.7140	0.7288

5. CONCLUSIONS

This mathematical analysis investigates the influence of rheological parameters such as yield stress, maximum stenosis depth, flow index, thickness of peripheral layer, stenosis length ratio etc. on the rheological measurements such as velocity distribution, shear stress at the blood vessel wall, rate of flow, flow impedance, slip velocity and viscosity of fluid in the blood flow through small diameter blood vessels, treating the blood as two-phase H-B fluid model. Analytical solutions to the aforesaid flow quantities are obtained and MATLAB codes are developed to generate the data for plotting graphs and also to present them in the tabular form to quantify the variations in the aforesaid rheological quantities. The main outcomes of this study are collated below:

- Velocity of blood increases significantly when the flow index parameter n and stenosis length ratio β increase.
- When the stenosis length ratio β and the flow index parameter n increase, the slip velocity soars and an opposite behavior is noticed for the core fluid's viscosity when the aforesaid parameters increase.
- Rate of flow and velocity of blood rise when the Reynolds number Re_p increases.
- When the maximum stenosis depth increases, the rate of flow falls considerably while the wall shear stress and flow impedance increase significantly.
- When the yield stress of blood increases, the slip velocity and the shear stress at the blood vessel wall increase appreciably.
- The percentage of difference between the core fluid's viscosity in two-phase H-B fluid flow model and the experimental values in the blood vessel's diameter $40\ \mu m$ and $66.6\mu m$ are 1.27% and 0.32% respectively and the corresponding difference observed by Ponalagusamy and Tamil Selvi [30] for two-phase fluid Casson fluid model are 3.75% and 6.86%.
- The aforesaid percentage of difference is considerably lower for the two-phase H-B fluid model compared to that of two-phase Casson fluid model.
- The estimates of the slip velocity of the two-phase H-B fluid model in the blood vessels of diameter $40\ \mu m$ and $66.6\mu m$ are 1.202 and 0.7405 respectively and these values are in close agreement with the corresponding values obtained by Ponalagusamy and Tamil Selvi [30] for two-fluid Casson model.
- The estimates of the core fluid's viscosity in two-phase H-B fluid model increases gradually with the increase of flow index parameter in the blood vessels of diameter $40\ \mu m$ and this behavior is reversed in the blood vessels of diameter $66.6\mu m$.
- When the core fluid's viscosity rises, the estimates of the slip velocity decreases rapidly in the blood vessel of diameter $40\ \mu m$ and it increase marginally in the blood vessels of diameter $66.6\mu m$.

Since the present theoretical study brings out several interesting results and also provides some possible clinical applications, it is expected that the results of present study shall be useful to medical practitioners to predict the blood flow behavior in stenosed blood vessels. Since atherosclerosis is a major cardiovascular disease leading to human death, the present results may be useful to surgeons to decide whether a patient with a particular depth of arterial constriction should undergo a surgery or can the subject be treated through medication itself. This study shall further be extended by incorporating the additional parameters such as the presence external body vibrations, magnetic field and also assuming the blood vessel wall to have the characters of porosity and permeability.

ACKNOWLEDGEMENT

This research did not receive any specific grant from funding agencies in the public, commercial, ornot-for-profit sectors.

CONFLICT OF INTEREST

The authors confirm that there are no known conflicts of interest associated with this publication and there has been no significant financial support for this work that could have influenced its outcome.

REFERENCES

[1] D. F. Young, F. Y. Tsai. 1973. Flow characteristic in models of arterial stenosis-I, steady flow, J. Biomech. 6: 395-410.

[2] D. F. Young. 1979. Fluid mechanics of arterial stenosis, J. Biomech. Eng. Trans. ASME. 10: 157-175.

[3] R. Ponalagar Samy. 1986. Blood Flow through Stenosed Tube, IIT, Bombay, India, Ph.D thesis.

[4] D. Liepsch, M. Singh, L. Martin. 1992. Experimental analysis of the influence of stenotic geometry on steady flow. Biorheology. 29: 419-431.

[5] P. Chaturani, R. Ponnalagar Samy. 1986. Pulsatile flow of Casson's fluid through stenosed arteries with applications to blood flow, Biorheology. 23: 499-511.

[6] S. Chakravarty, A. Datta. 1989. Effects of stenosis on arterial rheology through a mathematical model. Math. Comp. Model. 12: 1601-1612.

[7] R. Ponalagusamy, S. Priyadharshini. 2017. Nonlinear model on pulsatile flow of blood through a porous bifurcated arterial stenosis in the presence of magnetic field and periodic body acceleration. Computer Methods and Programs in Biomedicine. 142: 31-41.

[8] T. Karino, H. L. Goldsmith. 1977. Flow behavior of blood cells and rigid spheres in annular vortex, Philos. Trans. R. Soc. London. B279: 413-445.

[9] J. N. Kapur. 1992. Mathematical Models in Biology and Medicine, East-West Press Pvt. Ltd., New Delhi, India. pp. 368-369.

[10] K. G. Mann, S. Butenas, K. Brummel. 2003. The dynamics of thrombin formation, Arteroscler. Thromb. Vasc. Biol. 23: 17.

[11] V. P. Srivastava. 2007. A theoretical model for blood flow in small vessels, Appl. Appl. Math. 2: 51-65.

[12] J. B. Shukla, R. S. Parihar, B. R. P. Rao. 1980. Effects of stenosis on non-Newtonian flow of blood in an artery, Bull. Math. Biol. 42: 283-294.

[13] K. Vajravelu, S. Sreenadh, P. Devaki., K. V. Prasad. 2011. Mathematical model for a Herschel-Bulkley fluid flow in an elastic tube, Cent. Eur. J. Phys. 9: 1357 - 1365.

[14] D. S. Sankar and A. I. M. Ismail. 2010. Effects of periodic body acceleration in blood flow through stenosed arteries – a theoretical model, Int. J. Nonlinear Sci. Num. Simul. 11: 243-257.

[15] P. Chaturani, R. Ponnalagar Samy. 1985. A study of non-Newtonian aspects of blood flow through stenosed arteries and its applications in arterial diseases, Biorheology. 22: 521-531.

[16] C. Tu, M. Deville. 1996. Pulsatile flow of non-Newtonian fluids through arterial stenosis. J. Biomech. 29: 899-908.

[17] D. S. Sankar. 2011. Two-phase non-linear model for blood flow in asymmetric and axisymmetric stenosed arteries. Int. J. Non-Linear Mech. 46: 296-305.

[18] V. P. Srivastava, M. Saxena. 1994. Two-layered model of Casson fluid flow through stenotic blood vessels: Applications to cardiovascular system. J. Biomech. 27: 921-928.

[19] N. Santhosh, G. Radhakrishnamacharya. 2016. A two-fluid model for Herschel-Bulkley fluid flow through narrow tubes. J. Appl. Sci. Eng. 19: 241-248.

[20] D. S. Sankar, U. Lee. 2007. Two-phase non-linear model for the flow through stenosed blood vessels. J. Mech. Sci. Tech. 21: 678-689.

[21] W. A. Hyman. 1973. The role of slip in the rheology of blood. Biorheology. 10: 57-60.

[22] Y. Nuber. 1971. Blood flow, slip and viscometry, J. Biophys. 11: 252-264.

[23] N. Santhosh, G. Radhakrishnamacharya, A. J. Chamkha. 2015. Effect of slip on Herschel-Bulkley fluid flow through narrow tubes. Alexandria Engng. J. 54: 889-896.

[24] A. Zaman, N. Ali. 2016. Effects of peripheral layer thickness on pulsatile flow of Herschel-Bulkley fluid through a stenotic artery.Canadian J. Phys. 94: 920-928.

[25] A. Bhatnagar, R. K. Shrivastav, A. K. Singh. 2015. Effect of slip velocity on blood flow through composite stenosed arteries: A Herschel-Bulkley fluid model. Nat. Acad. Sci. Let. 38: 251-255.

[26] J. C. Misra, G. C. Shit. 2007. Role of slip velocity in blood flow through stenosed arteries: A non-Newtonian model. J. Mech. Med. Biol. 7: 337-353.

[27] D. S. Sankar, U. Lee. 2006. Influence of slip velocity in Herschel-Bulkley fluid flow between parallel plates - A mathematical study. J. Mech. Sci. Tech. 30: 3203-3218.

[28] V. P. Srivastava, R. Rastogi, R. Vishnoi. 2010. A two-layered suspension blood flow through an overlapping stenosis. Comp. Math. Appl. 60: 432-441.

[29] C. Y. Wong, James Bassingthwaighte. 2003. Blood flow in small curved tubes. J. Biomech. Engng. 125: 910-913.

[30] R. Ponalagusamy, R. Tamil Selvi. 2011. A study on two-layered model (Casson-Newtonian) for blood flow through an arterial stenosis: Axially variable slip velocity at the wall. J. Franklin Institute. 348: 2308-2321.

[31] P. Brunn. 1975. The velocity slip of polar fluids, Rheol. Acta 14: 1039-1054.

[32] G. Bugliarello, J. W. Hayden. 1963. Detailed characteristics of the flow of blood in vitro, Trans. Soc. Rheol. 7: 209-230.

[33] G. Bugliarello, J. Sevilla. 1970. Velocity distribution and other characteristics of steady and pulsatile blood flow in fine glass tubes. Biorheology. 7: 85-107.